ARTICLE

Modulating Cell Adhesion Dynamics on Carbon Nanotube Monolayer Engineered with Extracellular Matrix Proteins

Ning Cai,[†] Chee C. Wong,[†] Ying X. Gong,[†,‡] Samuel C. W. Tan,[†] Vincent Chan,[†] and Kin Liao*[,†]

School of Chemical and Biomedical Engineering, Nanyang Technological University, Singapore 639798, and Institutes of Life and Health Engineering, Jinan University, Guangzhou, P.R. China 510632

ABSTRACT Although it has been demonstrated that carbon nanotubes (CNTs) may have potentials for tissue engineering applications because of their unparalleled physical properties, little has been known on the cell adhesion mechanisms on model CNT monolayer pertaining to the design of novel cell therapeutics device. In this study, the adhesion dynamics of primary porcine esophageal fibroblasts (PEFs) on CNT monolayer were elucidated with confocal reflectance interference contrast microscopy (C-RICM) integrating with phase contrast microscopy. Moreover, CNT monolayer (CNT-ML) was functionalized with two typical extracellular matrix (ECM) proteins including collagen type I (COL) and fibronectin (FN) in order to promote its biocompatibility. First, it is shown by atomic force microscopy that the topographical features of CNT-ML were dependent on the types of immobilized ECM protein. Second, significant time lag in adhesion contact evolution (around 10 min) for PEFs was found on both CNT-ML and CNT-COL compared to the negligible time lag on CNT-FN. It was found that adhesion energy of PEFs on the CNT-COL and CNT-FN surfaces reached steady state at 60 and 30 min after cell seeding compared to 70 min on CNT-ML surface. At steady state, the adhesion energy of PEFs on the CNT-COL and CNT-FN surfaces was about twice as much than that on the CNT-ML surface. Moreover, immobilization of collagen or fibronectin on CNT monolayer led to an increase in seeding efficiency and proliferation rate of PEFs. Scanning electron microscopy and immunostaining together demonstrated that PEFs displayed an elongated morphology and highly polarized actin network on both CNT-COL and CNT-FN surfaces, whereas PEFs displayed nonuniform cell morphology and actin organization on the CNT-ML surface. Overall, our results demonstrated that the biophysical responses and biological behavior of PEFs on unmodified or functionalized CNT monolayer were different. Functionalization of CNT through extracellular matrix protein immobilization effectively promotes cell adhesion and proliferation, which may provide information for designing CNT-based biomaterials or novel cell therapeutics devices in biomedical engineering.

KEYWORDS: carbon nanotube • cell adhesion • adhesion dynamics • surface functionalization

1. INTRODUCTION

Carbon nanotubes (CNTs), cylindrical macromolecules of carbon with unique, unparallel mechanical, electrical, and thermal properties, were discovered in 1991 (1). Because of their unique physical properties, CNTs are potentially useful in a wide variety of applications, such as electronics, optics, and advanced materials (2, 3). Recently, CNTs have also stimulated immense interest in their potential applications in biomedical devices (4). For example, the unique properties of CNTs, such as a large surface area to volume ratio and high mechanical strength, make them an excellent candidate for providing the needed structural reinforcement for tissue engineering scaffolds (5–8). Although there is a concern about cytotoxicity of CNT (9–12), several published studies supported the biocompatibility of CNT and CNT-based biomaterials (13–16). Furthermore, the toxicity of CNT can be possibly mitigated through functionalization with biological molecules (5, 17, 18).

The aim of tissue engineering is "... development of biological substitutes that restore, maintain, or improve tissue function or a whole organ," according to Langer and Vacanti (19). Therefore, the design of successful engineered tissue requires thorough understanding of the interaction between cells and tissue transplant (20). The effective adhesion of cell to biomaterial surface is an indispensable requirement for designing any engineered tissue equivalent (21). Functionalization of biomaterials with extracellular matrix (ECM) proteins has been proven to be useful for improving the biocompatibility of biomaterials for cell regeneration (22). Generally, it is known that ECM proteins immobilized on biomaterial surface convey both mechanical and chemical stimuli into the adhering cell, and in turn induce cytoskeleton remodeling, morphology transformation and gene expression (23). Thus it is natural to hypothesize that ECM protein functionalization would promote cell adhesion to CNT or CNT-based composite biomaterials. CNTs can be functionalized with various biomolecules including ECM proteins with or without chemical coupling (24). The large aromatic (π-electrons) surface of CNTs makes it easy for biomolecules to bind through hydrophobic interac-

* To whom correspondence should be addressed. Tel: (65)6790-5835. Fax: (65)67911761. E-mail: askliao@ntu.edu.sg.
Received for review November 21, 2009 and accepted March 10, 2010
[†] Nanyang Technological University.
[‡] Jinan University.
DOI: 10.1021/am9008117

Published on Web 03/23/2010

tions (25). After introducing the biomolecular ligands onto CNTs, it is possible to enhance the biorecognition of cells and promote cell adhesion onto CNTs. For instance, MacDonald et al. reported design of collagen—CNT composite materials as potential scaffolds in tissue engineering (6). However, the lack of quantitative understanding on the effect of ECM protein immobilization on the adhesion mechanism of cells on CNTs becomes a hurdle for the development of CNT-based biomaterials.

Cell adhesion to biomaterials comprises three stages: cell attachment, cell spreading, and focal adhesion, as well as stress fiber formation (26). Conventional methods including phase contrast microscopy and fluorescence microscopy are employed to study cell morphology and the focal adhesion formation. Recently, confocal reflectance interference contrast microscopy (C-RICM) has emerged as an ideal real-time imaging technique for probing the interfacial contact zone between cell and biomaterial (27). By integrating C-RICM with conventional microscopy, the adhesion kinetics of HepG2 on different engineered surfaces has been elucidated (28–30). To date, little is known on the interactions between cells and CNT-based surfaces in quantitative sense, thus more comprehensive studies are needed for a thorough understanding on related issues; this is particularly important for specific cell types for specific applications, such as esophagus tissue engineering.

Esophagus cancer is one of the most common cancers. Replacement of the cancerous esophagus by engineered tissue equivalent is considered an ideal treatment in the future. However, there is currently a lack of focus on the development of novel materials for enabling esophagus regeneration. One of the key tasks of esophageal tissue engineering is to develop biofunctional materials that can for tissue regeneration for esophagus substitute; CNT-based biomaterials could be one of the solutions. To date, study on the adhesion behavior of primary esophageal cells on CNT-based material is scarce. The primary objective of this study is to quantitatively elucidate adhesion dynamics of primary porcine esophageal fibroblasts (PEFs) on CNT monolayer with a combination of unique biophysical approaches. First, collagen type I (COL) and fibronectin (FN), two key ECM proteins, were immobilized on CNT monolayer through physical adsorption. Several physical parameters, (i) the initial rate of cell deformation, (ii) steady-state degree of deformation, and (iii) adhesion energy of PEFs on neat or ECM protein-immobilized CNT monolayer during initial cell seeding, were determined. It is shown by the results that the biophysical parameters of cell adhesion can be tuned significantly by immobilization of biomolecules. Moreover, cell seeding efficiency and proliferation activity were correlated to the adhesion dynamics on various CNT-based materials. In addition, fluorescence microscopy and scanning electron microscopy (SEM) were used to examine actin filament distribution and degenerated structures of PEFs, respectively.

2. EXPERIMENTAL SECTION

2.1. Materials. Dulbecco's modified eagle medium (DMEM), penicillin-streptomycin solution, fetal bovine serum (FBS), and trypsin-EDTA were obtained from Invitrogen (USA). Phosphate buffer saline, collagen type I (bovine), fibronectin (bovine), QuantiPro bicinchoninic acid (BCA) assay kit, MTT solution, glutaraldehyde, and paraformaldehyde, were all purchased from Sigma-Aldrich Chemical Inc. (USA). The CNT monolayers supported on glass substrate were obtained from Nanolab biosystem Inc. (USA).

2.2. Substrate Preparation. The CNT monolayer used in our study was a layer of multiwalled carbon nanotubes (MWCNTs) covalently bound to a silica coverslip. Before usage, each coverslip with CNT monolayer was thoroughly washed by deionized water. Subsequently, the coverslip was dry by air and exposed to UV light for 30 min. Collagen type I or fibronectin solution (0.6 mg/mL in 1× PBS) was dispensed onto the CNT monolayer followed by incubation for 24 h at 4 °C. Finally, the coverslip was washed three times with 1× PBS to remove unbound collagen or fibronectin. For convenience, CNT monolayer, collagen-coated CNT monolayer, and fibronectin-coated CNT monolayer are abbreviated as CNT-ML, CNT-COL, and CNT-FN, respectively, hereafter.

The density of immobilized collagen or fibronectin was determined by QuantiPro BCA assay kit (31). In brief, the protein-coated substrates were immersed in 1% sodium dodecyl sulfate (SDS) and shaken for 30 min to desorb the immobilized proteins. The desorbed protein solution was then transferred into a centrifuge tube and QuantiPro BCA working reagent was added to the tube with protein solution, followed by gentle mixing. After incubation for 2 h at 37 °C, the sample was cooled down to room temperature and its absorbance was measured at 562 nm with UV—visible spectrophotometer (Shimadzu UV-2450, Shimadzu Corp., Japan). The amount of proteins adsorbed on each surface was calculated based on standard curves made from each individual protein. Each measurement was run in triplicate.

2.3. Atomic Force Microscopy. The topographical feature of the CNT based material was examined by a NanoMan AFM (Vecco Inc., USA) with tapping mode. A cantilever with a spring constant of 0.03 N/m was used to scan an area of 1 μm in dimension for each sample. Each AFM image is a representation of at least three scans collected from each type of surface. All AFM images were analyzed by AFM associated software to determine the root-mean-square (rms) roughness.

2.4. Contact Angle Measurement. The contact angle of distilled water (18.2 MΩ) on CNT based surfaces was measured by the sessile drop technique using a contact-angle measurement equipment (FTA 1000, First Ten Angstroms Inc., USA) at room temperature. Water droplets of 5 μL formed by an automatic microsyringe were dropped onto different points of each surface, and the image of attached droplet was record after 30 s. Water contact angle was obtained by analyzing the image of the droplet. Eight or more measurements were carried out and the mean values were calculated.

2.5. Porcine Esophageal Fibroblast Culture. Primary porcine esophageal fibroblasts (PEFs) were isolated and cultured according to a previously reported method (32). Following isolation, PEFs were incubated in DMEM, supplemented with 10% heat-inactivated FBS, 100 U/ml penicillin, and 100 U/ml streptomycin at 37 °C in 5% CO_2 atmosphere. Upon 80—90% confluence, cells were harvested for subculturing or experiments using trypsin-EDTA solution. The cells used for all experiments were controlled between passage 6 and passage 10.

2.6. Phase Contrast Microscopy and Confocal Reflection Interference Contrast Microscopy. The details of (inverted) phase contrast microscopy and C-RICM have been described previously (27). These two techniques were used to visualize the contour of adherent cells and their adhesion contact, respectively. Strong adhesion contact of an adherent cell appears as a dark or light gray region in the gray background on the C-RICM image. A Pascal 5 confocal microscope system (Carl

Zeiss, Germany) was used for imaging the adherent cells on CNT-ML or ECM protein functionalized CNT-ML. After cell seeding, a series of phase contrast and C-RICM images were taken at regular intervals. Throughout the experiment, the cells were kept at 37 °C and 5% CO_2 through a customized chamber (Carl Zeiss, Germany). Using an image analysis software (ZSM5, Carl Zeiss, Germany), the midplane radius of adhering cells (R) and contact zone radius (a) were obtained. The degree of deformation, α, is defined as $\alpha = a/R = \sin\theta$. On the basis of a mechanical model of adherent cells, the adhesion energy is given by (33)

$$w = (1 - \cos\theta)C\varepsilon + C\varepsilon^2 \quad (1)$$

where ε, average biaxial strain of cell membrane, is expressed in terms of α:

$$\varepsilon = \frac{1}{2}\left[\frac{2 + 2(1 - \alpha^2)^{1/2}}{4/R_1^2 - \alpha^2} - 1\right] \quad (2)$$

and C, proportionality constant of the cell membrane, is calculated by

$$C = \frac{Eh}{1 - v} \quad (3)$$

In eq 3, v and h are Poisson ratio and membrane thickness, respectively. Elastic modulus of porcine esophageal fibroblast, E, is taken as 12 kN/m^2 according to the reported result by AFM indentation (34).

2.7. Cell Seeding Efficiency Assay. Cell seeding efficiency is defined as the ratio of the number of adherent cells to original number of seeded cells. Before each assay, cells were seeded onto the different substrates. Following 24 h of cell culture, the substrates were washed and the adherent cells were detached with trypsin-EDTA. The numbers of seeded cells and adherent cells were counted with a hemocytometer. Each assay was run in triplicate for each of the three surfaces.

2.8. MTT Assay. MTT assay was carried out to investigate proliferation activity of PEFs. This assay is based on the cleavage of tetrazolium ring of MTT by mitochondrial dehydrogenases of viable cells, yielding purple formazan crystals that are insoluble in aqueous solutions. Briefly, PEFs at the seeding density of 1×10^5 cells/cm^2 were cultured on three different types of substrates for 1 or 3 days. In the last 4 h of each culture period, cells were covered with 1 mg/mL of MTT solution. Following 4 h of incubation, the MTT solution was removed and the specimen was washed with 1× PBS. The formazan crystals produced were dissolved in dimethyl sulfoxide and a microplate reader (GENios, Tecan Inc., USA) was used to measure the absorbance at a wavelength of 570 nm. Each test was repeated three times for each surface.

2.9. Scanning Electron Microscopy. The detailed morphology of the cells was examined by scanning electron microscopy (SEM). First, cells seeded on different substrate (CNT-ML, CNT-COL and CNT-FN) were cultured for 24 h. Then the substrates with adherent cells were rinsed with 1× PBS followed by fixation with 2.5% glutaraldehyde (SEM grade) for 2 h. After three rinses with 1× PBS, the specimens were immersed in 1% osmium tetroxide solution for 1 h. The fixed specimen were dehydrate with a graded ethanol series (30, 50, 70, 90, 95, 2 × 100%) for 10 min at each concentration, soaked in hexamethyldisilazane for 10 min, and dried in air. Finally, the specimens were sputtered with a layer of platinum and visualized by a field emission SEM (JSM-6700, JEOL Ltd., Japan).

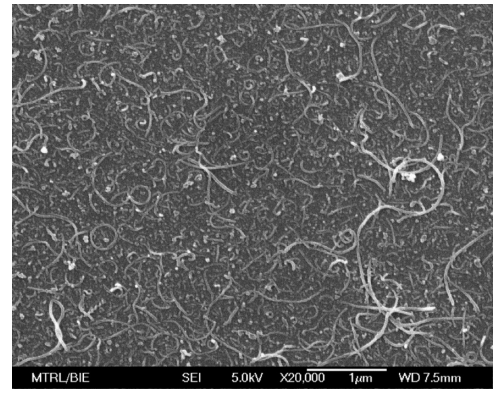

FIGURE 1. SEM image of CNT monolayer on a silica coverslip.

The SEM images were analyzed using AxioVision, an image analysis software (Carl Zeiss, Germany). After measuring spread area and perimeter of cells, we calcualted the cell shape factor coefficient (Sfc) (35), defined as $4\pi \times$ (spread area)/(perimeter^2). Sfc ranges from 0 to 1, where 0 implies a straight line, and 1 denotes circular shape.

2.10. Immunofluorescence Staining. To visualize actin filaments, we cultured PEFs on three surfaces for 24 h. The cells was then washed in 1× PBS, fixed in 4% paraformaldehyde solution for 30 min, washed again in 1× PBS, and stained with FITC-labeled phalloidin (5 μg/mL) for 40 min. Finally, the samples were washed in 1× PBS to remove residual stain and viewed using confocal laser scanning microscope (Pascal 5, Carl Zeiss, Germany).

2.11. Statistical Analysis. All data are shown as mean ± standard deviation. A one-way ANOVA was performed to compare mean values among different groups. Probability values of $p < 0.05$ were considered statistically significant.

3. RESULTS AND DISCUSSION

3.1. Surface Characterization. A typical SEM image of unmodified CNT monolayer supported on glass substrate is shown in Figure 1. The result shows that long, curly MWCNTs with length of 1.7 ± 0.8 μm are randomly distributed on the substrate. The diameters of MWCNTs are in the range of 20 to 40 nm, with average value of 27.4 nm. In addition, it is seen that these MWCNTs protrude from the bottom of the coverslip and their frontal parts may overlap. Thus the thickness of the monolayer varies slightly across the substrate.

Proteins can be immobilized onto CNT by spontaneous adsorption or chemical reactions (24). Although protein immobilization onto CNT via chemical reaction may be carried out in a more controllable way, protein coating through physical adsorption remains to be common practice due to its simplicity (24). Because of the hydrophobic nature of CNT surface, collagen or fibronectin can nonspecifically bound to the wall of CNT through noncovalent bonding. AFM height and phase images of CNT-ML, CNT-COL and CNT-FN surfaces are shown in Figure 2. The peak of a surface is represented as bright region in an AFM phase image. It is shown in images A and B in Figure 2 that CNTs with different length protrude from the coverslip. Compared to Figure 2A, the CNT-COL surface shown in Figure 2C is relatively flat. However, some very bright regions are observed in Figure

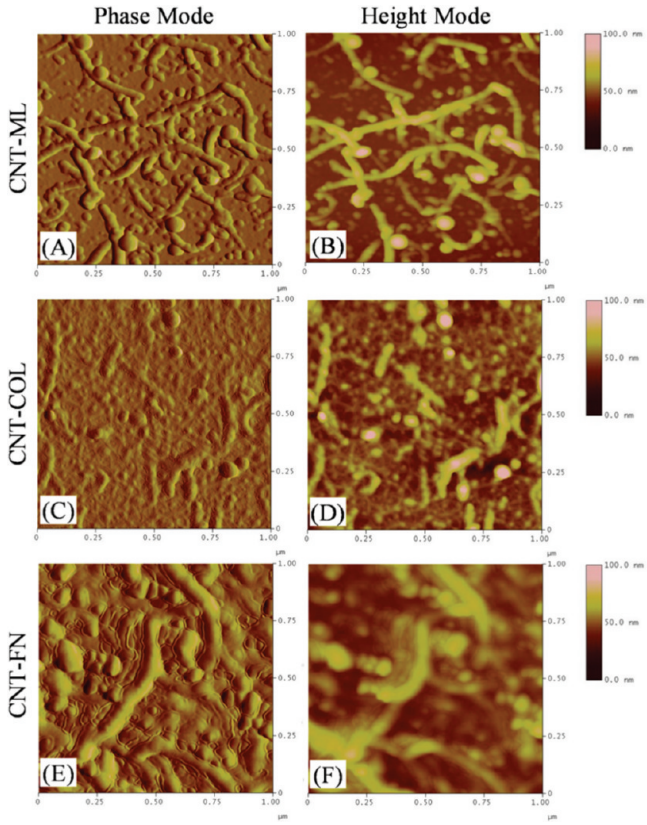

FIGURE 2. AFM images of CNT-ML, CNT-COL, and CNT-FN surfaces.

2D, suggesting that some CNTs are exposed outside the protein layer. After collagen immobilization, the ridges between tangled CNTs are filled with collagen, leading to a more homogeneous morphology as shown in the phase image of the CNT-COL surface than that of the CNT monolayer. As shown in images E and F in Figure 2, similar topographic features are also found on the CNT-FN surface. However, the fibronectin layer on the CNT-FN surface is not as smooth as the collagen layer on the CNT-COL surface, possibly attributed to the higher molecular weight of fibronectin (approximately 450 kD) compared to collagen (approximately 300 kD), and because of differential tertiary organizational capacities of the proteins. By analyzing the topographic images of the three surfaces, the root-mean-square (rms) roughness of CNT-ML, CNT-COL, and CNT-FN surfaces are 9.45 ± 1.32, 4.55 ± 0.31, and 6.23 ± 0.42 nm, respectively ($p < 0.05$). ECM immobilization leads to a decrease in rms roughness compared to neat CNT monolayer, which confirms successful ECM immobilization onto the CNT monolayer.

Functionalization of CNT monolayer may induce change of its hydrophobic nature due to the introduction of ECM proteins. Contact angles of CNT-ML, CNT-COL, and CNT-FN surfaces are 120.6 ± 3.0, 53.3 ± 2.2, and $93.1 \pm 1.5°$, respectively ($p < 0.01$). The contact angle of CNT monolayer was found to be significantly higher than those of CNT-COL and CNT-FN surfaces, exhibiting the innate hydrophobic nature of carbon nanotubes. Because of the immobilization of collagen, the CNT-COL surface became more hydrophilic. In contrast, the CNT-FN surface was still somewhat hydrophobic. It was previously reported by Harnett et al. that fibronectin-coated surface retained hydrophobic nature and was independent of the underlying substrates (36). Our result is consistent with their finding. By QuantiPro BCA measurement, the densities of absorbed collagen on CNT-COL surface and fibronectin on CNT-FN surface were determined to be 2.14 ± 0.26 and 2.38 ± 0.31 $\mu g/cm^2$ (which is statistically insignificant, with $p > 0.05$), respectively. The result showed that both proteins formed multiple molecular layer on CNT since the required density for forming a collagen or fibronectin monolayer is 0.30 and 0.25 $\mu g/cm^2$, respectively (29, 37). Thus the amount of immobilized ECM proteins on CNT-ML is believed to be sufficient for enhancing cell adhesion.

3.2. Adhesion Dynamics of PEFs on CNT-ML, CNT-COL, and CNT-FN Surfaces. Cell attachment and spreading are phenotypic responses of all anchorage-dependent cells (26). Using C-RICM in conjunction with phase contrast microscopy, adhesion contact and spreading area can be monitored simultaneously, which provides succinct descriptions of cell geometry on a planar substrate. A series of phase contrast and C-RICM images of a typical PEF on the CNT-ML surface during 2 h of culture is shown in Figure 3. The result shows that the PEF maintains round shape within 40 min after cell seeding on CNT-ML. After 2 h of culture, the PEF begins to spread with filopodia protruding from cellular membrane. It has been shown that cell spreading was shown to be decoupled from the adhesion contact development in the initial phase of cell adhesion (38). Thus C-RICM provides additional information about cell adhesion mechanism. As demonstrated in the C-RICM images of Figure 3, the PEF forms strong adhesion contact at 20 min after cell seeding as represented by a light gray patch with an area of 31 μm^2 in the C-RICM image (indicated by the white arrow in Figure 3). The gray patch significantly increases in area over time. After 120 min of culture, the adhesion contact area reaches 296 μm^2. By comparing the phase contrast images with C-RICM images within 40 min, it is found that the evolution of adhesion contact is different from that of cell spreading. The contact area of PEF at 40 min is 204 μm^2, 560% higher than that of PEF at 20 min. In contrast, the projected area of PEF retains almost constant at about 310 μm^2 during the initial 40 min of culture. Despite the lack of adhesive ligand, CNT-ML is effective at inducing adhesion contact formation. The result observed herein is likely caused by rapid adsorption of serum proteins on CNT-ML by hydrophobic interaction. In fact, the first stage of cell adhesion (cell attachment) is mainly driven by binding of integrin receptors to the ligands on biomaterials (26), whereas the development of cell spreading is controlled by cytoskeleton remodeling (39). Although the ligand−receptor interactions trigger signal transduction cascades, the downstream biophysical responses, such as cytoskeleton reorganization, occur later than the adhesion contact evolution. This evidence supports the independent trend of adhesion contact evolution and cell spreading during the initial cell adhesion process.

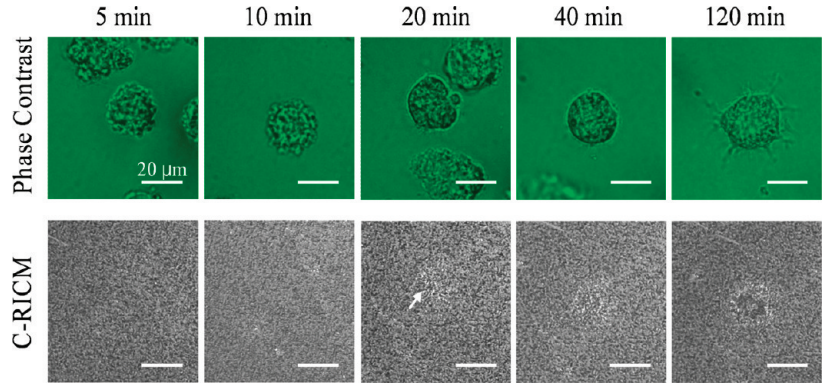

FIGURE 3. Series of phase contrast and C-RICM images of a typical PEF in a cell population adhering to the CNT-ML surface from 5 to 120 min after cell seeding. The white arrow indicates the adhesion contact forming at 20 min. Scale bar = 20 μm.

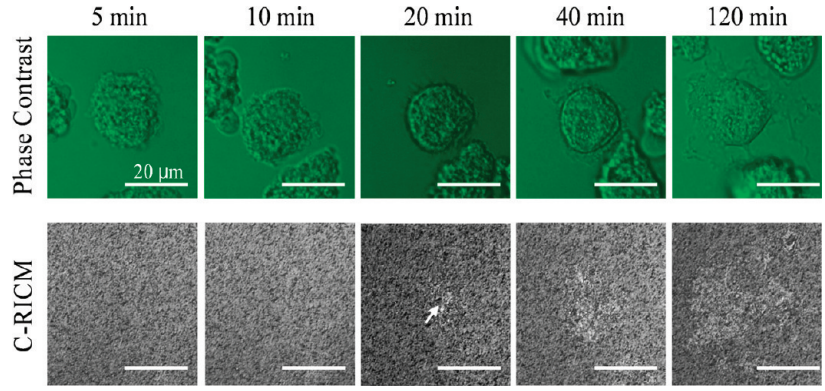

FIGURE 4. Series of phase contrast and C-RICM images of a typical PEF in a cell population adhering to the CNT-COL surface from 5 to 120 min after cell seeding. The white arrow indicates the adhesion contact forming at 20 min. Scale bar = 20 μm.

Immobilization of ECM protein on biomaterials provides necessary ligands for cell adhesion, which is critical to the long-term anchorage of seeded cells. A series of phase contrast and C-RICM images of a typical PEF on the CNT-COL surface are shown in Figure 4. From the phase contrast images, it is observed that a PEF displays round shape during the initial 40 min of cell seeding. At 40 min, the PEF spreads a little with filopodia formations near cell periphery, which is not found in PEF on CNT monolayer at the same time of observation. Through 2 h of culture, this PEF spreads extensively. Lamellipodia and filopodia are seen to protrude from the cell membrane. As indicated in the C-RICM images of Figure 4, the PEF initiates its adhesion contact formation (indicated by the white arrow in Figure 4) 20 min post seeding. Thereafter, the adhesion contact area climbs up from 58 μm^2 at 20 min to 785 μm^2 at 120 min. The result implies that the interaction between the integrin receptors of PEF and immobilized collagen accelerates adhesion contact formation compared to that for PEF on CNT-ML.

Switching one ECM protein to another alters ligand–receptor interactions, which may induce a shift of downstream signal transductions inside the adherent cells. A series of phase contrast and C-RICM images of a typical PEF on the CNT-FN surface are shown in Figure 5. The cell goes through the significant filopodia formation and extensive spreading in 2 h of culture, which is similar to the PEF on the CNT-ML or CNT-COL surface. However, there is a notable distinction between the evolution of adhesion contact of PEFs on the CNT-FN surface compared to that of PEFs on the CNT-ML or CNT-COL surface. Just 5 min after cell seeding, a dark patch (as indicated by the white arrow in Figure 5), with an area of 91 μm^2 emerges on the CNT-FN surface. This faster adhesion contact formation of PEFs to the CNT-FN surface than that on the CNT-ML and CNT-COL demonstrates better biorecognition of fibronectin by PEFs. Moreover, the density of adsorbed fibronectin is close to that of collagen. It is because fibronectin contains abundant types of binding domains including Arg-Gly-Asp (RGD) and Arg-Glu-Asp-Val (REDV) (20), which may favor more rapid identification and binding of transmembrane integrin receptors of PEFs to the immobilized fibronectin. From 5 to 120 min, the contact zone grows quickly. After 2 h of culture, the contact area reaches 1288 μm^2, which is the biggest for PEFs at 120 min among all of the three surfaces. In our previous adhesion dynamics results of PEFs on poly(lactic acid) (PLA), collagen-functionalized PLA (PLA-COL), and fibronectin-functionalized PLA (PLA-FN) surfaces, PEFs on the PLA-FN surface also exhibit the fastest adhesion contact formation among three cases (38). These results support the notion that adhesion contact development is modulated by the interactions between immobilized ECM protein and cellular receptors in the CNT system.

Cell adhesion always induces cell deformation through the geometric transformation. The degree of deformation, a/R, which characterizes the geometric change during cell adhesion, can be obtained conveniently by our biophysical approaches. The average degree of deformation (a/R) against seeding time for PEFs on three surfaces (CNT-ML, CNT-COL,

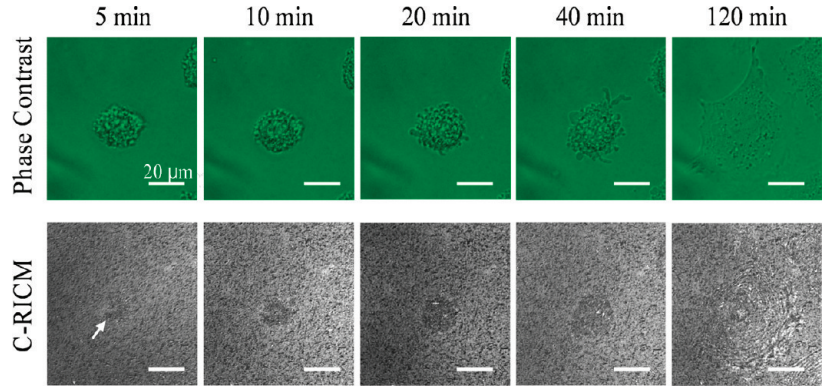

FIGURE 5. Series of phase contrast and C-RICM images of a typical PEF in a cell population adhering to the CNT-FN surface from 5 to 120 min after cell seeding. The white arrow indicates the adhesion contact forming at 5 min. Scale bar = 20 μm.

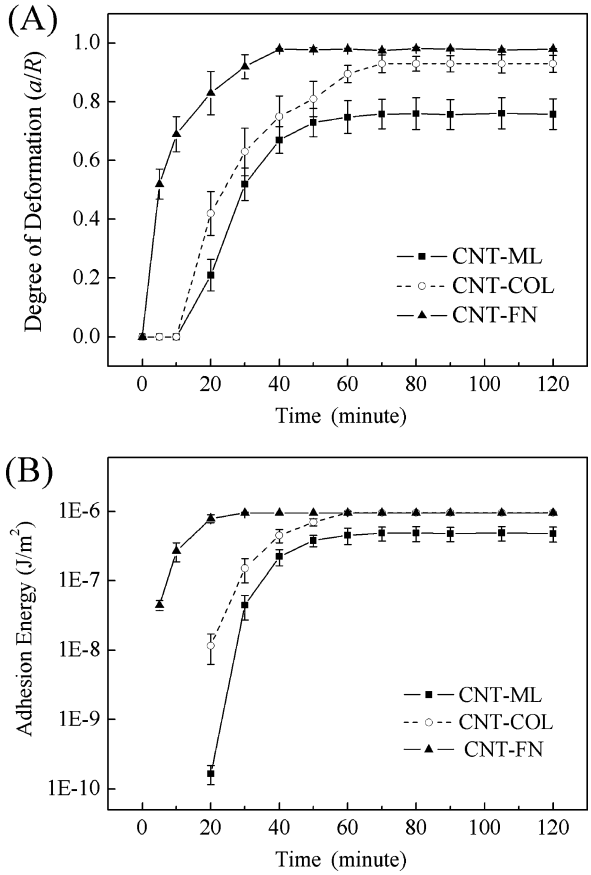

FIGURE 6. (A) Average degree of deformation and (B) average adhesion energy versus time for PEFs on CNT-ML, CNT-COL and CNT-FN surfaces within 2 h after cell seeding. $n > 50$ for each data point.

and CNT-FN) during 2 h culture is shown in Figure 6A. It is demonstrated that *a*/*R* of PEFs on CNT-ML surface retains zero within the initial 10 min of cell seeding. Moreover, the average increase rate of *a*/*R* is defined as deformation rate that is *a*/*R* divided by the time needed for the cells during initial stage of adhesion contact formation. At 20 min, *a*/*R* obtains a value of 0.21 (with deformation rate of 0.021 min^{-1}). The rate of increase of average *a*/*R* against time is gradually slackened from 30 min onward. At 80 min, *a*/*R* acquires its maximum value on CNT-ML. Similarly, *a*/*R* of PEFs on CNT-COL surface remains to be zero within 10 min followed by the rapid rise from 20 min (with deformation rate of 0.042 min^{-1}). However, the trend of *a*/*R* against time for PEF on the CNT-FN surface is largely different from those of the other two surfaces. From 0 to 5 min, *a*/*R* of PEFs on CNT-FN surface jumped from 0 to 0.52 (with deformation rate of 0.1 min^{-1}). The lag time for PEFs to initiate adhesion to CNT-FN surface is 15 min shorter than that of CNT-ML and CNT-COL surfaces, which may be attributed to the quicker recognition of fibronectin by integrin receptors of PEFs based on the indifference in the density of adsorbed collagen and fibronectin. After 40 min, *a*/*R* of PEFs on CNT-FN surface reaches the maximum value. The result strongly indicates that the evolution of cell adhesion contact on CNT-FN surface is most rapid and has the highest deformation rate among the three surfaces reported herein. Different pairs of ligands and receptors may modulate the adhesion contact dynamics of PEF cells. In particular, the integrin receptors on most anchorage dependent cells play a critical role in several cellular processes including tissue morphogenesis, organogenesis, tumor metastasis (22). It is known that integrin $\alpha_5\beta_1$ specifically recognizes fibronectin and subsequently triggers ECM remodelling (22). Moreover, collagen is one of the major ECM proteins containing a lot of cell binding sites such as RGD sequences. Integrin $\alpha_2\beta_1$ mediates the adhesion of cell to collagen and is closely associated with intracellular signal transduction (30). The results herein demonstrates the clear role of ligand−receptor interaction in dictating the initial adhesion kinetics of PEF cells.

Through 2 h of culture, PEFs on three surfaces reach a steady state and gain their maximum value of *a*/*R*. The maximum *a*/*R* of PEFs on CNT-ML, CNT-COL, and CNT-FN surfaces is 0.76, 0.93, and 0.98, respectively ($p < 0.05$). For spreading cells, *a*/*R* is translated into the ratio of the radius of adhesion contact zone to the radius of spreading portion. The maximum *a*/*R* value for PEFs on CNT-COL and CNT-FN surfaces is almost 1, suggesting major spreading membrane of cells is tightly bound to the substrates because of ECM immobilization. The result also shows that CNT-ML alone is not optimized for cell activation.

Adhesion energy is a useful biophysical parameter describing the binding affinity between adherent cells and biomaterials surfaces (40). The average adhesion energy of PEFs against time of cell seeding, calculated using eq 1, on

CNT-ML, CNT-COL, and CNT-FN surfaces during 2 h culture is shown in Figure 6B. For all three surfaces, the adhesion energy of PEFs goes up over time until reaching their steady state. Because the zero value would not appear in log scale, the average adhesion energy of cells on CNT-ML and CNT-COL surfaces before 20 min is not shown in Figure 6B, implying no formation of strong adhesion contact for PEFs on CNT-ML and CNT-COL surfaces before 20 min. The average adhesion energy of PEFs on CNT-ML surface climbs up from 1.66×10^{-10} J/m^2 at 20 min to 4.86×10^{-7} J/m^2 at 70 min, spanning 3 orders of magnitude. During the same culture period, it only spans about 2 orders of magnitude on CNT-COL surface, from 1.16×10^{-8} J/m^2 to 9.54×10^{-7} J/m^2. For PEFs on CNT-FN surface, high adhesion energy with 4.45×10^{-8} J/m^2 shows up only at 5 min after cell seeding. It then keeps on rising and reaches a steady state of 9.54×10^{-7} J/m^2. The time needed for PEFs on CNT-ML, CNT-COL, and CNT-FN surfaces to reach maximum adhesion energy is 70, 60, and 30 min, respectively. The adhesion energy PEFs on CNT-FN surface spend the least time to arrive at the steady state. In our previous study, PEFs on ECM protein-functionalized PLA surfaces followed a similar trend to gain the maximum adhesion energy over time (38). These results suggest immobilized ECM proteins may act as major mediator of cell adhesion (23).

3.3. Seeding Efficiency and Proliferation Activity of PEFs on CNT-ML, CNT-COL, and CNT-FN Surfaces. Cell seeding efficiency assay was carried out to characterize the global affinity of biomaterial surfaces to PEFs. It is indicated in Figure 7A that seeding efficiency of PEFs on CNT-ML, CNT-COL and CNT-FN surfaces after 2 h of culture is 32 ± 11, 68 ± 6, and 83 ± 7%, respectively ($p < 0.05$). Through the introduction of ECM protein as ligands onto CNT monolayer, the seeding efficiency was elevated approximately 2-fold. Particularly, PEFs on CNT-FN surfaces possess the highest seeding efficiency among the three cases, demonstrating that fibronectin immobilization enhances cell adhesion most effectively among the three cases. A similar effect of ECM immobilization on seeding efficiency was found on PLA-COL and PLA-FN surfaces in our previous studies (38).

An MTT assay was conducted to monitor the variation of cell number in 3 days of culture. Data shown in Figure 7B are represented in the form of relative values to the control surface (CNT-ML, 1 day). As shown in Figure 7B, cell number of PEFs on CNT-COL and CNT-FN surfaces was significantly higher than that on CNT-ML surface after either 1 day or 3 days of culture according to the linear correlation between cell number and MTT value. This result agrees well with published studies of myoblastic mouse cells (C2C12) cultured on unmodified or FBS-functionalized carbon nanotube films (41).

To systematically investigate cell proliferation activity, we integrated cell seeding efficiency data with MTT results for analysis. The ratios of cell number on CNT-ML, CNT-COL, and CNT-FN surfaces are deduced to be 1:2.1:2.6 (2 h), 1:2.5:3.0 (1 day), and 1:2.7:3.2 (3 days), respectively. Obviously,

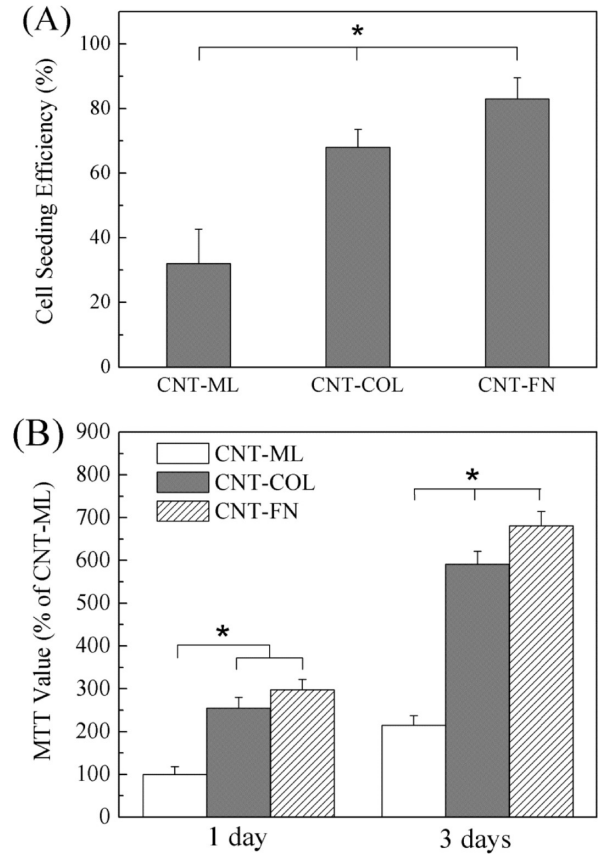

FIGURE 7. (A) Cell seeding efficiency of PEFs on CNT-ML, CNT-COL, and CNT-FN surfaces after 24 h of culture. (B) MTT value for PEFs cultured on CNT-ML, CNT-COL, and CNT-FN surfaces after 1 or 3 days of culture. * Represents significant difference among the groups for comparison ($p < 0.05$); in A and B (3 days), the comparison is among all of the three groups; in B (1 day), the comparison is between CNT-ML and CNT-COL, and CNT-ML and CNT-FN.

the ratio of cell number on CNT-COL or CNT-FN surface to that on CNT-ML surface increases steadily from 2 h to 3 days, demonstrating PEFs proliferates more quickly on ECM protein functionalized surfaces. By considering the different seeding efficiency on three surfaces, proliferation rate is defined as MTT value of 3 days divided by that of 1 day to compare cell proliferation activities in absence of the effect of seeding efficiency. The proliferation rate of PEFs on CNT-ML, CNT-COL, and CNT-FN surfaces is 2.07, 2.36*, and 2.33*, respectively (* $p < 0.05$, compared to CNT-ML surface), suggesting immobilization of ECM protein accelerates proliferation activity of PEFs. Therefore, higher cell number on functionalized CNT monolayer than that on CNT-ML surface could be attributed to the enhancement of both seeding efficiency and proliferation rate through engineering the CNT-ML surface with ECM proteins.

3.4. Cell Morphology of PEFs on CNT-ML, CNT-COL, and CNT-FN Surfaces. Cell morphology under high resolution are intimately related to many physiological processes, including cell growth, differentiation and apoptosis (42). In our experiments, PEFs cultured on different surfaces for 24 h were fixed, dehydrated, and then observed under SEM to examine their morphology. SEM images of PEFs adhering to CNT-ML, CNT-COL and CNT-FN surfaces are shown in Figure 8. On the CNT-ML surface, the morphol-

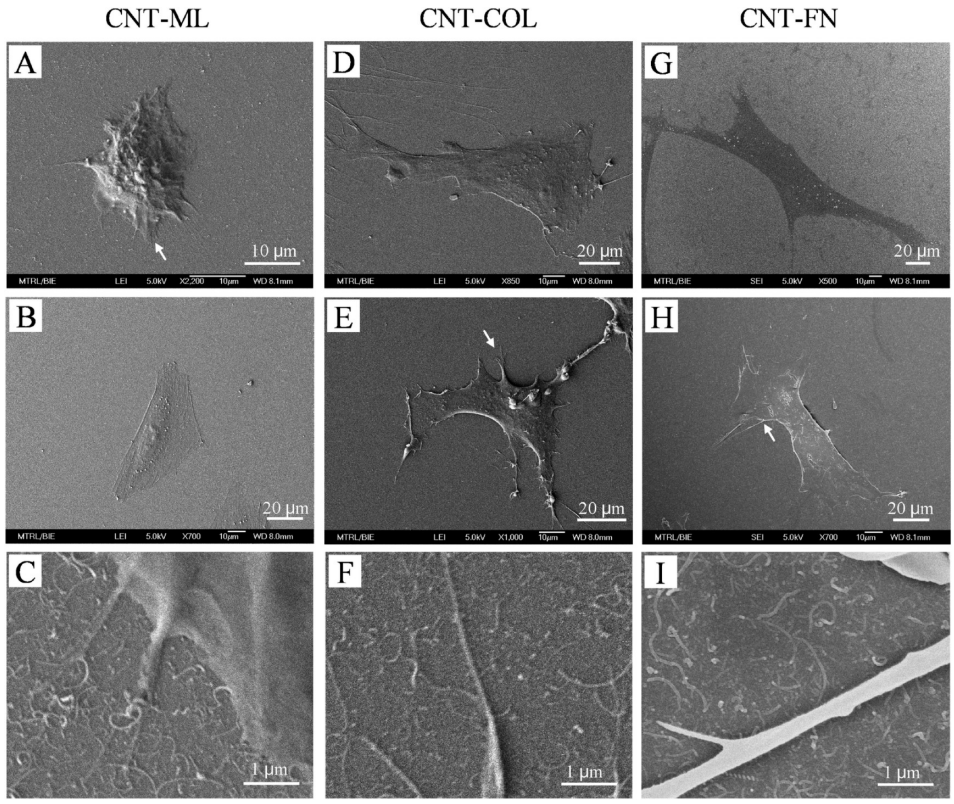

FIGURE 8. SEM images of PEFs adhering to CNT-ML, CNT-COL, and CNT-FN surfaces after 24 h of culture. The arrows in A, E, and H indicate the filopodia of a typical PEF on CNT-ML, CNT-COL and CNT-FN surfaces, respectively. The corresponding details of the filopodia in A, E, and H are shown in C, F, and I, respectively.

ogy of cells is not uniform: Some cells are almost circular, whereas others are polygonal. As shown in Figure 8A, the cell spreads slightly and exhibits a relatively round shape. In contrast, the cell as shown in Figure 8B significantly spreads and display elongated morphology. It is known that anchorage-dependent cells rely on spreading to enter G1 and G2 of the cell cycle (43). It was found that cells which only bound to ECM and lacked spreading did not elevate cyclin D1 level and downregulate the cell-cycle inhibitor p27 (44), suggesting PEFs with nearly round morphology on the CNT-ML surface may not proliferate normally. Comparatively, the morphology of PEFs on CNT-COL or CNT-FN surface is uniform. In Figure 8D, E, G, and H, all cells display highly elongated morphology. The details of filopodia of a typical PEF on CNT-ML, CNT-COL and CNT-FN surfaces are shown in Figure 8C, F, and I, respectively. It is depicted in these figures that filopodia sprawl on the CNT sidewalls. On multiwalled CNT construct, other researchers noticed that filopodia of human osteoblastic cells grasped and deformed the surrounding compliant CNTs (45). No similar phenomena were found in our study. A possible explanation is that CNTs on our substrate are shorter. Under the same load, the deflection of shorter CNTs is so small that it is unnoticeable under SEM.

To quantitatively compare the different morphology of cells on three surfaces, spread area and shape factor coefficient (Sfc) of cells are determined by analyzing the SEM images. Spread area and Sfc of PEFs on the three surfaces after 24 h of culture are listed in Table 1. These two parameters are used to evaluate the degree of cell spreading and cell elongation, respectively. The lower the Sfc value for a cell, the more elongated its morphology. It is indicated in Table 1 that spread area of cells on CNT-COL and CNT-FN surfaces is bigger than that on CNT-ML surface. In contrast, Sfc of cells on CNT-COL and CNT-FN surfaces is lower that on CNT-ML surface. The functionalization of CNT-ML with ECM proteins modulates the morphology of adherent cells. For instance, cells adhering on functionalized CNT monolayer possess larger spread area and more elongated morphology than those on unmodified CNT monolayer. Particularly, cells on CNT-FN surface display most expanded and elongated morphology among the three surfaces, very similar to the bipolar morphology of PEFs in vivo. The difference in cell morphology on three surfaces reflects the variation of ligand−receptor interactions, which tune cell morphology. It is worth emphasizing that inconsistency of cell morphology was not found on biofunctionalized CNT monolayer. A possible explanation was related to the improved uniformity of the surface chemistry through functionalization. It was reported that spread area of human osteoblastic cells cultured on CNT construct was negatively correlated with

Table 1. Spread Area and Sfc of PEFs on CNT-ML, CNT-COL, and CNT-FN Surfaces

surfaces	spread area*(μm^2)	Sfc*
CNT-ML	1326 ± 594	0.81 ± 0.10
CNT-COL	2456 ± 467	0.67 ± 0.07
CNT-FN	2886 ± 536	0.62 ± 0.05

* Significant difference in spread area or Sfc between PEFs on three types of surfaces ($p < 0.05$). $n = 50-60$ for each data point.

nanotube diameter (45). The diameters of CNTs on CNT-ML surface used herein ranged from 20 to 40 nm. The dissimilar cellular shape and spread area for cells on the CNT-ML surface may just act as the mirror of underlying CNTs with different size. On the CNT-COL and CNT-FN surfaces, the ECM protein layer encapsulating the CNT sidewalls possible insulates the effect of size of CNT on cell morphology. In our previous studies, PEFs also exhibited more spread area and elongated morphology on PLA-FN surface than PLA and PLA-COL surfaces (38). These results supports that immobilized ligands, not the underlying supporting materials mainly dictates the resulted phenotypes of adherent cells.

3.5. Actin Filament Distribution of PEFs on CNT-ML, CNT-COL, and CNT-FN Surfaces. Cell adhesion to biomaterials triggers signal transduction cascades, inducing cytoskeleton reorganization. The change of biomaterial surface may lead to alteration of signal transduction pathways and cytoskeleton organization of adherent cells. In present study, F-actin was immunostained by FITC-phalloidin to observe the actin filament organization. Representative images of stained PEFs on three surfaces after 24 h of culture are shown in Figure 9. It is found in Figure 9A that the F-actin distribution in PEFs on CNT-ML surface is not consistent. There are two types of actin organization on CNT-ML surface: one is in the less-spreaded cells (indicated by the white arrows in Figure 9A), with concentrated actin filaments near cell cortex; the other is in well-spread cells, with actin filament bundles appearing all over the cytosol. In the former case, actin microfilament bundles are not observed. Only the randomly oriented actin filaments near cell cortex form a roughly ringlike structure correlating with its nearly round shape. In contrast, no circular actin structure is found in the latter, but the cells exhibit clearly visible stress fibers. Functionalization of CNT monolayer affects the actin organization of adherent cells. Contrary to the CNT-ML, the distribution of F-actin inside various PEFs on the CNT-COL surface is more consistent in comparison with that on CNT-ML. As demonstrated in Figure 9B, PEFs spread extensively on CNT-COL surface. It is seen from the figure that cells are highly polarized on CNT-COL, with stress fibers (indicated by the white arrow) aligning parallel to the long axis of the cells, which indicates the presence of focal adhesion—although formation of focal adhesions may not necessarily warrant the formation of stress fibers. It can be inferred from these images that the number of focal adhesions for PEFs on CNT-COL are much more than those on CNT-ML. It is shown in Figure 9C that F-actin distribution of PEFs on CNT-FN surface is very similar to that on the CNT-COL surface. Highly anisotropic orientation of stress fibers are seen inside the highly polarized PEFs. Comparing the F-actin distribution of PEFs on the three surfaces, it is obvious that ECM protein immobilization on CNT monolayer has greatly transformed the diverse actin organizations of PEFs into consistent actin organization with parallel alignment of stress fibers, which demonstrated the critical role of immobilized ligands in modulating cell adhesion. The results of actin organization of PEFs on three surfaces coincide with the SEM observations.

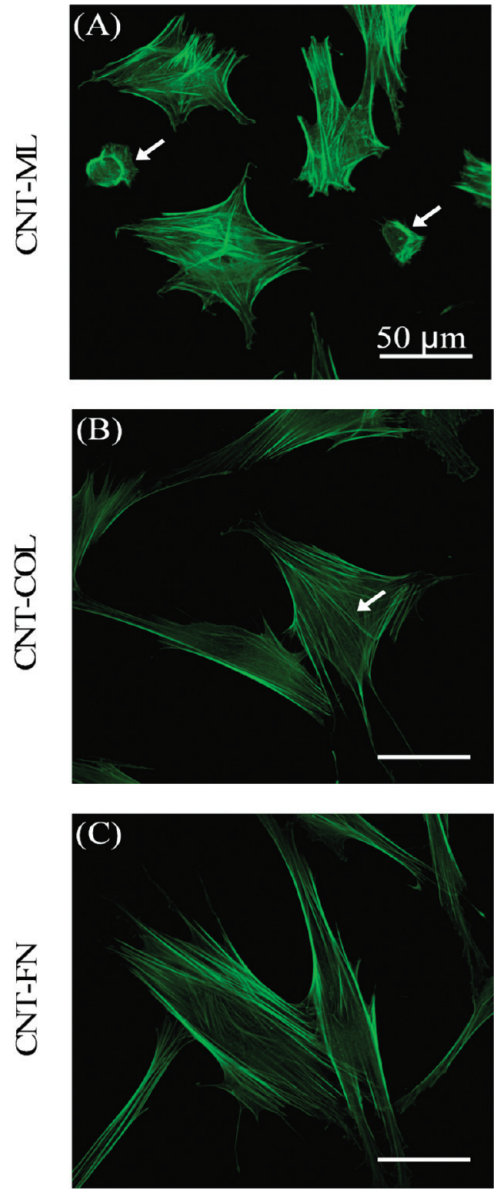

FIGURE 9. Actin filament distribution of PEFs on CNT-ML, CNT-COL, and CNT-FN surfaces after 24 h of culture. The arrows in A indicate less spread cells with concentrated actin filaments near cell cortex. The arrow in B indicates the stress fibers in spreading cells; similarly, stress fibers are also seen in C. Scale bar = 50 μm.

4. CONCLUSIONS

In summary, the adhesion dynamics of PEFs on CNT-ML surface and functionalized CNT-ML surfaces (CNT-COL and CNT-FN) was investigated. First, the effect of ECM immobilization on the interfacial properties of CNT-ML has been thoroughly characterized. It is shown that adhesion dynamics of PEFs on three surfaces is different. In general, a/R and adhesion energy for PEFs reach steady state more quickly on functionalized CNT-ML surfaces than on CNT-ML surface. Particularly, PEFs on the CNT-FN surface initiate adhesion contact formation and reach steady state earlier than that on CNT-COL surface, reflecting the different innate bioactive domains inside ECM proteins. Seeding efficiency and proliferation activity of PEFs were also elevated after functionalization of CNT-ML. The most prominent result in our study is that the inconsistent cell morphology and actin

organization on CNT-ML surface become uniform on functionalized CNT-ML surface. PEFs on CNT-FN surface possess the highest elongated morphology and largest spread area among three cases after 24 h culture. Thus, ECM protein functionalization effectively promotes PEF adhesion to the CNT monolayer. Engineering the CNT surface with ECM proteins provides a feasible way in designing optimized biomaterial surface for tissue engineering.

Acknowledgment. The authors acknowledge partial support of this project by the Singapore-University of Washington Alliance. We also acknowledge Dr. Ning Fang and Miss Alicia G. G. Toh for obtaining AFM images.

REFERENCES AND NOTES

(1) Iijima, S. *Nature* **1991**, *354*, 56–58.
(2) Baughman, R. H.; Zakhidov, A. A.; de Heer, W. A. *Science* **2002**, *297*, 787–792.
(3) Arnold, M. S.; Green, A. A.; Hulvat, J. F.; Stupp, S. I.; Hersam, M. C. *Nat. Nanotechnol.* **2006**, *1*, 60–65.
(4) Yang, W. R.; Thordarson, P.; Gooding, J. J.; Ringer, S. P.; Braet, F. *Nanotechnology* **2007**, *18*, 412001.
(5) Harrison, B. S.; Atala, A. *Biomaterials* **2007**, *28*, 344–353.
(6) MacDonald, R. A.; Laurenzi, B. F.; Viswanathan, G.; Ajayan, P. M.; Stegemann, J. P. *J. Biomed. Mater. Res., Part A* **2005**, *74A*, 489–496.
(7) Abarrategi, A.; Gutierrez, M. C.; Moreno-Vicente, C.; Hortiguela, M. J.; Ramos, V.; Lopez-Lacomba, J. L.; Ferrer, M. L.; del Monte, F. *Biomaterials* **2008**, *29*, 94–102.
(8) Shi, X.; Sitharaman, B.; Pham, Q. P.; Liang, F.; Wu, K.; Edward Billups, W.; Wilson, L. J.; Mikos, A. G. *Biomaterials* **2007**, *28*, 4078–4090.
(9) Jia, G.; Wang, H. F.; Yan, L.; Wang, X.; Pei, R. J.; Yan, T.; Zhao, Y. L.; Guo, X. B. *Environ. Sci. Technol.* **2005**, *39*, 1378–1383.
(10) Lam, C. W.; James, J. T.; McCluskey, R.; Arepalli, S.; Hunter, R. L. *Crit. Rev. Toxicol.* **2006**, *36*, 189–217.
(11) Cui, D. X.; Tian, F. R.; Ozkan, C. S.; Wang, M.; Gao, H. J. *Toxicol. Lett.* **2005**, *155*, 73–85.
(12) Soto, K.; Garza, K. M.; Murr, L. E. *Acta Biomater.* **2007**, *3*, 351–358.
(13) Smart, S. K.; Cassady, A. I.; Lu, G. Q.; Martin, D. J. *Carbon* **2006**, *44*, 1034–1047.
(14) Schipper, M. L.; Nakayama-Ratchford, N.; Davis, C. R.; Kam, N. W. S.; Chu, P.; Liu, Z.; Sun, X. M.; Dai, H. J.; Gambhir, S. S. *Nat. Nanotechnol.* **2008**, *3*, 216–221.
(15) Jell, G.; Verdejo, R.; Safinia, L.; Shaffer, M. S. P.; Stevens, M. M.; Bismarck, A. *J. Mater. Chem.* **2008**, *18*, 1865–1872.
(16) Usui, Y.; Aoki, K.; Narita, N.; Murakami, N.; Nakamura, I.; Nakamura, K.; Ishigaki, N.; Yamazaki, H.; Horiuchi, H.; Kato, H.; Taruta, S.; Kim, Y. A.; Endo, M.; Saito, N. *Small* **2008**, *4*, 240–246.
(17) Mattson, M. P.; Haddon, R. C.; Rao, A. M. *J. Mol. Neurosci.* **2000**, *14*, 175–182.
(18) Matsumoto, K.; Sato, C.; Naka, Y.; Kitazawa, A.; Whitby, R. L. D.; Shimizu, N. *J. Biosci. Bioeng.* **2007**, *103*, 216–220.
(19) Langer, R.; Vacanti, J. P. *Science* **1993**, *260*, 920–926.
(20) Shin, H.; Jo, S.; Mikos, A. G. *Biomaterials* **2003**, *24*, 4353–4364.
(21) Liu, C. Z.; Czernuszka, J. T. *Mater. Sci. Technol.* **2007**, *23*, 379–391.
(22) Wilson, C. J.; Clegg, R. E.; Leavesley, D. I.; Pearcy, M. J. *Tissue Eng.* **2005**, *11*, 1–18.
(23) Lebaron, R. G.; Athanasiou, K. A. *Tissue Eng.* **2000**, *6*, 85–103.
(24) Lin, Y.; Taylor, S.; Li, H. P.; Fernando, K. A. S.; Qu, L. W.; Wang, W.; Gu, L. R.; Zhou, B.; Sun, Y. P. *J. Mater. Chem.* **2004**, *14*, 527–541.
(25) Katz, E.; Willner, I. *Chemphyschem* **2004**, *5*, 1085–1104.
(26) Murphy-Ullrich, J. E. *J. Clin. Invest.* **2001**, *107*, 785–790.
(27) Chan, V.; Wan, K. T. *Langmuir* **2002**, *18*, 3134–3141.
(28) Yin, C.; Liao, K.; Mao, H. Q.; Leong, K. W.; Zhuo, R. X.; Chan, V. *Biomaterials* **2003**, *24*, 837–850.
(29) Tan, W. J.; Teo, G. P.; Liao, K.; Leong, K. W.; Mao, H. Q.; Chan, V. *Biomaterials* **2005**, *26*, 891–898.
(30) Feng, Z. Q.; Chen, W. N.; Lee, P. V. S.; Liao, K.; Chan, V. *Biomaterials* **2005**, *26*, 5348–5358.
(31) Cai, N.; Wong, C. C.; Tan, S. C. W.; Chan, V.; Liao, K. *Langmuir* **2009**, *25*, 10939–10947.
(32) Zhu, Y. B.; Chian, K. S.; Chan-Park, M. B.; Mhaisalkar, P. S.; Ratner, B. D. *Biomaterials* **2006**, *27*, 68–78.
(33) Wan, K. T.; Liu, K. K. *Med. Biol. Eng. Comput.* **2001**, *39*, 605–608.
(34) Rotsch, C.; Jacobson, K.; Radmacher, M. *Proc. Natl. Acad. Sci. U.S.A.* **1999**, *96*, 921–926.
(35) Allen, L. T.; Tosetto, M.; Miller, I. S.; O'Connor, D. P.; Penney, S. C.; Lynch, I.; Keenan, A. K.; Pennington, S. R.; Dawson, K. A.; Gallagher, W. M. *Biomaterials* **2006**, *27*, 3096–3108.
(36) Harnett, E. M.; Alderman, J.; Wood, T. *Colloids Surf., B* **2007**, *55*, 90–97.
(37) Goodman, S. L.; Cooper, S. L.; Albrecht, R. M. *J. Biomed. Mater. Res.* **1993**, *27*, 683–695.
(38) Cai, N.; Gong, Y.; Chian, K. S.; Chan, V.; Liao, K. *Biomed. Mater.* **2008**, *3*, 015014.
(39) Schoenwaelder, S. M.; Burridge, K. *Curr. Opin. Cell Biol.* **1999**, *11*, 274–286.
(40) Moy, V. T.; Jiao, Y. K.; Hillmann, T.; Lehmann, H.; Sano, T. *Biophys. J.* **1999**, *76*, 1632–1638.
(41) Li, X. M.; Gao, H.; Uo, M.; Sato, Y.; Akasaka, T.; Feng, Q. L.; Cui, F. Z.; Liu, X. H.; Watari, F. *J. Biomed. Mater. Res., Part A* **2009**, *91A*, 132–139.
(42) Huang, S.; Ingber, D. E. *Exp. Cell Res.* **2000**, *261*, 91–103.
(43) Folkman, J.; Moscona, A. *Nature* **1978**, *273*, 345–349.
(44) Huang, S.; Ingber, D. E. *Nat. Cell Biol.* **1999**, *1*, E131–E138.
(45) Mwenifumbo, S.; Shaffer, M. S.; Stevens, M. M. *J. Mater. Chem.* **2007**, *17*, 1894–1902.

AM9008117